ARTICLE IN PRESS

Available online at www.sciencedirect.com

ScienceDirect

International Journal of Rock Mechanics & Mining Sciences ▮ (▮▮▮▮) ▮▮▮–▮▮▮

International Journal of Rock Mechanics and Mining Sciences

www.elsevier.com/locate/ijrmms

Numerical study of flow anisotropy within a single natural rock joint

A. Giacomini[a,*], O. Buzzi[b], A.M. Ferrero[a], M. Migliazza[a], G.P. Giani[a]

[a]*Department of Civil and Environmental Engineering and Architecture, Università degli Studi di Parma, 43100 Parma, Italy*
[b]*Centre for Geotechnical and Materials Modelling, University of Newcastle, Callaghan, NSW 2308, Australia*

Received 2 August 2006; received in revised form 30 March 2007; accepted 2 April 2007

Abstract

The paper investigates the flow anisotropy within a natural joint subjected to mechanical shear. The cubic law is the simplest way to describe fluid flow through rock joints but because of rock wall roughness, deviations from this model have been observed. The Reynolds equation usually gives better results. In this study, micro-scale roughness is taken into account to define a reduced coefficient of permeability. Numerical simulations have been carried out by applying Darcy's law to the rock joint, described as an equivalent porous medium. The numerical simulations are based on experimental data obtained by Hans (PhD, Grenoble, 2002) from a series of hydromechanical shear tests on a rock joint replica. The numerical results have been compared to the experimental ones, and to the results obtained by applying the Reynolds equation, to assess the relevance of the simulations. For the fracture studied, the approach proposed herein can reproduce relatively well the experimental flow anisotropy, and provides consistent values of flow rates, whereas the Reynolds equation tends to give higher flow rates.

Keywords: Rock joints; Roughness; Flow anisotropy; Reduced permeability; Micro-scale; Cubic law; Shear test

1. Introduction

Understanding water flow through a rock mass is a fundamental issue in many areas of rock engineering, such as tunnel excavations, under the groundwater table, oil and gas reservoirs, underground nuclear waste disposal, or foundations in fractured rock masses. The flow through a discontinuous rock mass can be divided into flow through discontinuities and flow through the rock matrix. However, rock matrix permeability is often at least two orders of magnitude lower than rock joint permeability [1,2]. It can, therefore, be assumed that the flow is governed only by discontinuities, and it is thus of prime importance to fully understand their hydromechanical behaviour to foresee how stress fields in situ can influence the fluid transport through the fracture.

Many investigations have been performed over the past three decades on hydraulic and mechanical properties of natural rock joints and on the influence of external applied normal and shear stress [2–10]. The roughness of the rock walls has early been identified as a key parameter of the mechanical behaviour of rock joints [4,11]. Barton et al. [11] have proposed the JRC coefficient, an empirical parameter, to quantify the roughness but other approaches (e.g. geostatistical or fractal) have also been followed to quantify the roughness and its sensitivity to the scale [12–15].

The joint roughness governs the mechanical response of rock discontinuities, either in terms of stresses or displacements, as well as its hydromechanical behaviour. Indeed, an increased (or decreased) void space due to dilation (or contraction) will lead to an augmentation (or reduction) of the hydraulic conductivity. The roughness evolves significantly during a shear test [16,17] and several authors have studied the impact of the interface asperity degradation on the hydro-mechanical response [5,17–22] and on the alteration in hydraulic conductivity. If the fracture conductivity increases when rock wall asperities are worn off, it can also decrease when sheared rock particles close the flow path, which is known as the gouge material effect [22].

*Corresponding author. Tel.: +39 052 190 5709; fax: +39 052 190 5924.
E-mail address: anna.giacomini@unipr.it (A. Giacomini).

1365-1609/$ - see front matter © 2007 Elsevier Ltd. All rights reserved.
doi:10.1016/j.ijrmms.2007.04.007

Please cite this article as: Giacomini A, et al. Numerical study of flow anisotropy within a single natural rock joint. Int J Rock Mech Mining Sci (2007), doi:10.1016/j.ijrmms.2007.04.007

The flow through a rock fracture is governed by the Navier–Stokes equations, which are a set of three coupled non-linear equations difficult to solve. In case of a fracture bounded by smooth parallel walls, these former equations can be highly simplified and lead to the cubic law [23–25], which is still used in the literature in the rock joints context due to its simplicity (e.g., [26]) even if deviations from experimental data due to joint roughness have been observed [6,27,28]. Several attempts have been undertaken to improve the cubic law introducing roughness parameters [23,29–32] or reducing the value of the hydraulic aperture [19–21]. These corrections have not been that efficient and the main effect is a diminution of the total flow rate but the description of the flow anisotropy is poor. An equation more tractable than the Navier–Stokes equations and more accurate than the cubic law is the Reynolds equation, which is obtained by considerations of orders of magnitude [23,33]. So far, this equation is considered to describe properly the flow anisotropy within a rock joint [17,34].

This study intends to improve the description of flow anisotropy within a single discontinuity in an innovative way. The cubic law is combined to a reduction function taking into account the micro-scale roughness in order to define a reduced coefficient of permeability. This former is attributed to the elements constituting the rock joint, described as a porous medium in which Darcy's law is applied. The reduced coefficient of permeability at the micro-scale leads to a reorganization of flow towards most open channels. A good agreement between numerical results and experimental data after Hans [1] is thus obtained. In particular, flow anisotropy is well reproduced. A comparison with the Reynolds equation is given as well in order to highlight the efficiency of the model developed herein.

2. Experimental data

This study is based on the experimental data obtained by Hans [1] on the hydro-mechanical behaviour of rock joints under shearing. All experimental details are available in [1] and [35], especially the procedure to obtain the void map from the rock wall measurements. The chosen shear test (Test 1τ9) has been performed under a constant normal stress of 4 MPa and the relative tangential shear displacement, W, has been applied by successive steps of 2 mm until 10 mm. The anisotropy of the flow has been studied using an outlet membrane divided into five sectors (Fig. 1) and the morphology of both rock walls has been scanned with objective to build a map of the voids within the contact. Fig. 2 shows the lower rock wall in the (x,y,z) space at the initial step of the test. The laser used to obtain rock wall morphologies scans a series of parallel profiles with a constant step (0.6571 mm along the x-axis and 0.7 mm along the y-axis) and provides (x,y,z) coordinates of the scanned points. Then, both rock walls morphologies are matched using the normal and tangential displacements measurements (see details in [35]) and a void map at each stage of shearing can be obtained. This map represents the void space embedded within both rock walls and is used herein for the numerical simulations.

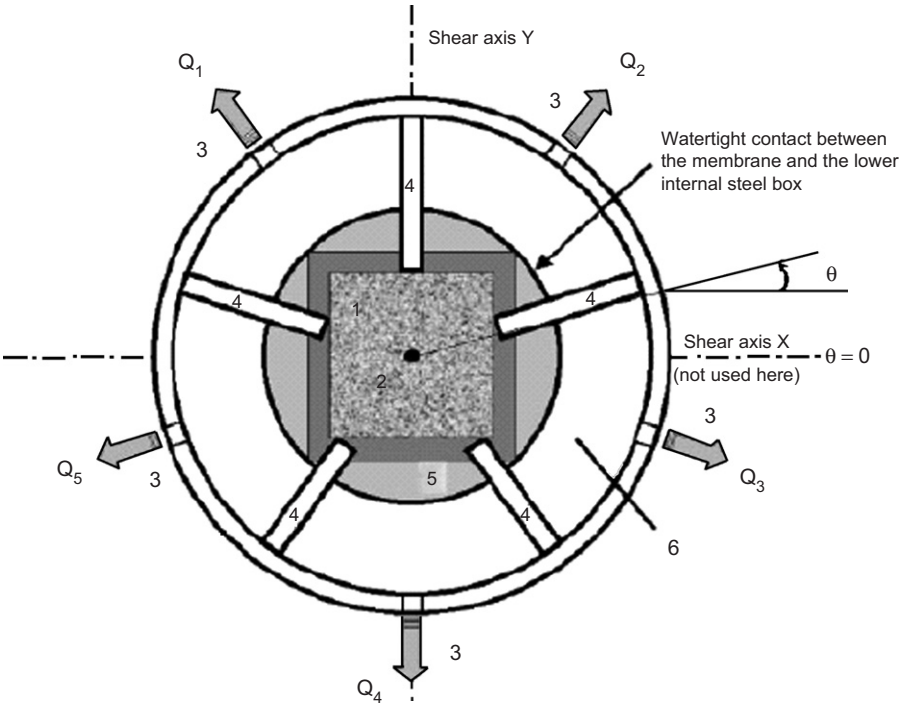

Fig. 1. Top view of the water-collecting membrane used for measuring flow anisotropy: 1, rock joint; 2, water inlet; 3, water outlet to the water mass measurement system; 4, wall for separation of the different sectors; 5, lower internal steel box; 6, collecting membrane (after [35]).

Please cite this article as: Giacomini A, et al. Numerical study of flow anisotropy within a single natural rock joint. Int J Rock Mech Mining Sci (2007), doi:10.1016/j.ijrmms.2007.04.007

3. Numerical model

The void space between joint walls is modelled as a fully saturated porous medium, of given coefficient of permeability, subjected to a pressure gradient reproducing the experimental conditions [35]. In such a medium, Darcy's law governs the flow and the pressure field. The void space embedded between both joint walls (70 mm wide per 70 mm long in the initial configuration; see Fig. 3) is described using eight-node brick elements (C3D8P elements) [36,37]. The total number of elements ranges from 7350 elements (for the maximum shear displacement of 10 mm) to a maximum value of 8715 elements (for the initial configuration, before shearing the rock joint). Indeed, the joint surface decreases from 70×70 to $70 \times 60\,\text{mm}^2$ during shearing test.

Regarding the boundary conditions, all (x,y,z) displacements are constrained. No flow is allowed through rock walls, external faces formed by the contour of both rock walls are subjected to atmospheric pressure, and all nodes of the central injection hole are subjected to the injection pressure (see Fig. 4a and b). The 3D FEM calculation code ABAQUS has been chosen to perform this study, since it can solve steady-state flows in a porous medium using Darcy's law, and thus calculate the effective pore fluid velocity. To study the flow anisotropy and to be able to compare the numerical results to the experimental ones, the outlet flow rate is quantified at the outlet of the joint in five sectors equivalent to the membrane divisions (see Results sections). The effective pore fluid velocity V_i is calculated at the integration points and its value is considered at the border elements to estimate the flow rate $Q_i = \vec{V}_i(S_i\vec{n}_i)$, where Q_i is the flow rate out of the boundary element i (section S_i orientated by the normal n_i) (Fig. 5). The total flow rate for each sector is the sum of the flow rates of the

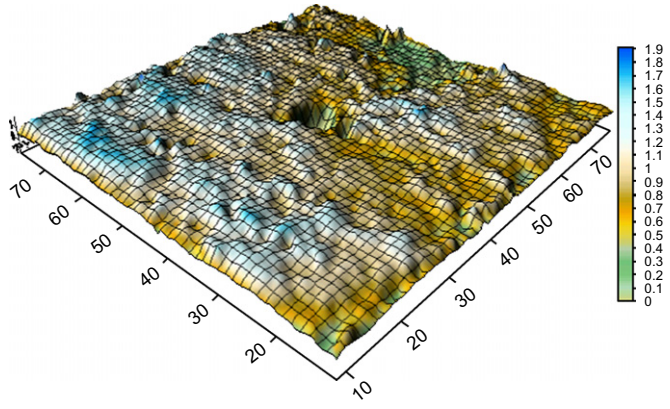

Fig. 2. 3D representation of the morphological analysis of the lower rock wall: initial configuration before shearing.

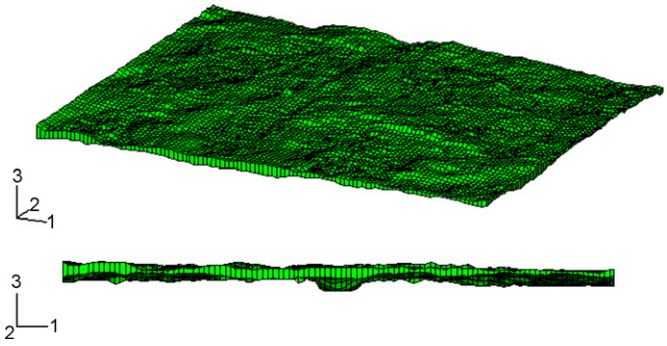

Fig. 3. 3D FEM representation of the void space embedded within both rock walls. Initial dimensions of the joint (before shearing): 70 mm × 70 mm. Final dimensions (end of the test): 70 mm × 60 mm.

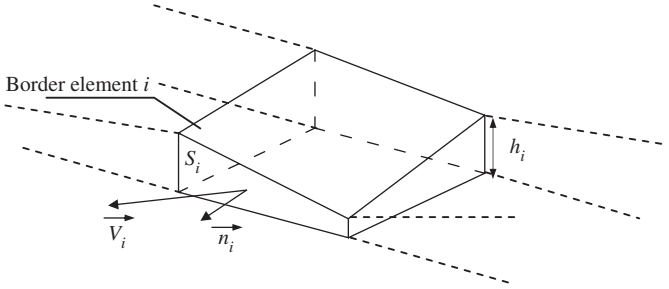

Fig. 5. Schematic representation of an element of the modelled void space and its edges. h_i: height of the edge. Estimation of the flow rate: $Q_i = \vec{V}_i(S_i\vec{n}_i)$ out of the border element i (section S_i orientated by the normal n_i).

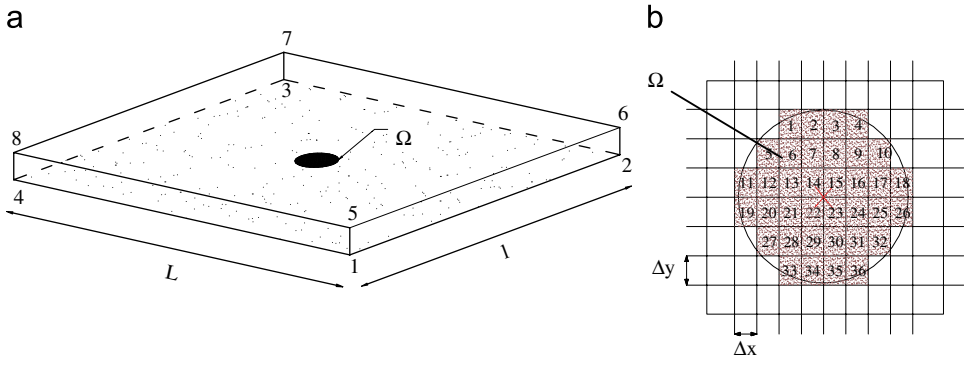

Fig. 4. (a) Simple parallel model for the boundary representation: faces 5678 and 1234 are impervious to the flow; faces 1265, 2376, 3487 and 1485 are at atmospheric pressure $P = 0$ MPa. Nodes on the Ω volume are at the injection pressure. L is equal to 70 mm, and l ranges from 60 mm to 70 mm. (b) Localization of injection hole drilled in the centre of the lower surface of the joint for the water injection and represented by the volume Ω.

Please cite this article as: Giacomini A, et al. Numerical study of flow anisotropy within a single natural rock joint. Int J Rock Mech Mining Sci (2007), doi:10.1016/j.ijrmms.2007.04.007

boundary elements of the sector. Five calculations are undertaken to reproduce the five shear steps of the hydro-mechanical test, from $W=2$ to 10 mm with a 2 mm increment.

Each element of the model is given a reduced coefficient of permeability defined as follows:

$$k_r = \frac{g e_{el}^2}{12v}\alpha(\Delta E_{el}/E_{el}), \quad (1)$$

where g is the gravitational acceleration, v is the kinematic viscosity of the fluid, e_{el} is the hydraulic aperture of the element and α is a reduction function taking into account the micro-roughness expressed by the ratio $\Delta E_{el}/E_{el}$. E_{el} is the mechanical aperture of the element and ΔE_{el} is the reduction of mechanical aperture. It can be noticed that $ge_{el}^2/12v$ corresponds to the coefficient of permeability given by the cubic law. The different steps of the reduced coefficient of permeability calculation are exposed in the following sections.

3.1. Micro-roughness quantification

A statistical analysis of the joint profile measurement made by Giacomini [38] is used herein. The joint is scanned by a series of profiles on x and y directions and, for each profile, the Z_2 parameter (root mean square of the first derivative of the profile) is evaluated. Tse and Cruden [13] have proposed a relation between the statistical operator Z_2 and the JRC for a step of 1.27 mm and Chiara [39] has extended this relation to other steps values. For a step corresponding to the distance between the two profiles, when scanning the rock wall (0.7 mm), the relation between $JRC_{profile}$ (roughness coefficient measured along a profile of the surface morphology) and Z_2 becomes:

$$JRC_{profile} = 25.75 + 25.04 \log Z_2. \quad (2)$$

The average joint roughness $\overline{JRC_0}$ is calculated as the average value of the profiles roughness (N is the total number of profiles):

$$\overline{JRC_0} = \frac{1}{N}\sum_{1}^{N} JRC_{profile}. \quad (3)$$

As shown in Fig. 6, no roughness data are given between two scanned points although the single element has its own roughness at the mineral scale. Hence, the joint roughness coefficient needs to be evaluated at the single finite element scale in order to better assess the differences between mechanical and hydraulic aperture. The empirical equation proposed by Bandis et al. [40], which is based on a large number of in situ and laboratory experiments, evaluates the JRC as

$$JRC = JRC_0\left(\frac{l}{l_0}\right)^{-0.02JRC_0}, \quad (4)$$

where JRC_0 is the laboratory scale roughness, l and l_0 are the lengths referring respectively to in situ scale and to the laboratory scale with $l > l_0$. This relation has already been used for $l < l_0$ by Giani et al. [41]. The authors have shown that, when studying the micro-scale, the joint roughness coefficient can be greater than 20 (maximum defined by Barton [11]). It can be noticed that this relation gives an infinite value of JRC when l tends to zero. However, if it makes sense to consider smaller scales (scale of particles or mineral cemented together and forming the rock wall, nugget effect), it does not make sense to reduce l indefinitely. Focusing on the micro-scale roughness herein, l_0 is still the laboratory size (about 70 mm) but l is the representative length of the model elements (0.7 mm). In this way, the joint roughness coefficient at element scale ($\overline{JRC_{el}}$) can be evaluated for each shear step. Table 1 shows the average roughness coefficient $\overline{JRC_0}$ (calculated from the rock wall morphology) and corresponding roughness coefficient of the element walls (micro-scale) $\overline{JRC_{el}}$ (calculated according to Eq. (4) with $l_0 = 70$ mm and $l = 0.7$ mm) for each displacement step W . Note that $\overline{JRC_{el}}$ is an average value and that JRC calculated at the element scale attains larger values than the laboratory scale JRC i.e. $\overline{JRC_{el}} > \overline{JRC_0}$.

Using the micro-scale roughness, $\overline{JRC_{el}}$ captures the fact that the elements have their own micro-scale roughness, which tends to reduce the flow. However, considering Fig. 7a and b, it appears the micro-scale roughness should not reduce the flow in the same proportions for elements of different height. To tackle this phenomenon, the reduction of mechanical aperture at micro-scale ΔE_{el} is introduced (see Fig. 8) in order to modify the coefficient of permeability calculation taking into account the ratio $\Delta E_{el}/E_{el}$. The micro-scale reduction of aperture has to be estimated from the macro-scale data since no data are

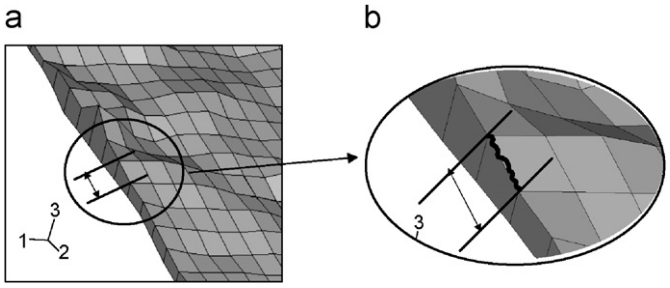

Fig. 6. FEM rock wall model: (a) view of the joint roughness (macro-scale) and (b) schematic representation of the element roughness (micro-scale) which is not taken into account in the FEM model.

Table 1
Steps of tangential displacement ($W=2$ to 10 mm) and corresponding average joint roughness coefficient ($\overline{JRC_0}$) and average element roughness coefficient ($\overline{JRC_{el}}$), calculated according to Eq. (4)

W (mm)	$\overline{JRC_0}$	$\overline{JRC_{el}}$
2	9.12	21.06
4	9.81	24.14
6	11.64	33.88
8	9.63	23.31
10	9.51	22.77

Please cite this article as: Giacomini A, et al. Numerical study of flow anisotropy within a single natural rock joint. Int J Rock Mech Mining Sci (2007), doi:10.1016/j.ijrmms.2007.04.007

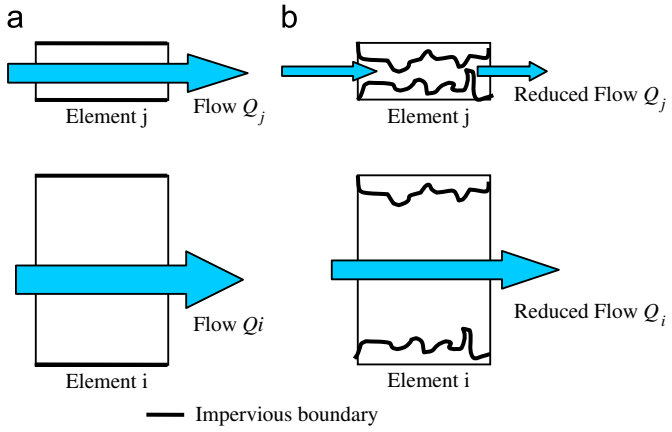

Fig. 7. Schematic representation of the flow within two elements without roughness and of different height: (a) smooth walls and (b) rough walls. The flow is not reduced in the same way for element j and i: flow within element j is much more affected by the roughness: $Q_i/Q_j < Q_{ri}/Q_{rj}$.

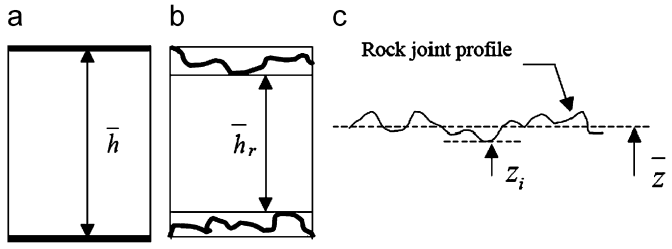

Fig. 8. (a) 2D schematic representation of an element of average height $\bar{h}$ and with smooth walls. (b) 2D schematic representation of an element of average height $\bar{h}$ and with micro-scale roughness. The equivalent smooth walls element has a reduced average height $\bar{h}_r$. The reduction of element height is defined as the reduction of mechanical aperture at the micro-scale: $\bar{h} - \bar{h}_r = \Delta E_{el}$. (c) Schematic representation of one profile of the rock joint, medium height $\bar{z}$ (obtained with x, y and z data) and height of each node z_i. $\Delta Z = \max(\bar{z} - z_i)$.

captured by the laser between the nodes. Fractal methods are commonly used to characterize rock joint roughness and self-affine figures are usually considered to better reproduce the joint roughness at different scale [14]. However, it is assumed herein that the maximum deviation from the average plane of the rock wall obeys a self-similarity law:

$$\left(\frac{\Delta Z}{l_0}\right)_{\text{macro}} = \left(\frac{\Delta Z_{el}}{l}\right)_{\text{micro}} \quad (5)$$

with $l_0 = 70$ mm for the joint, $l = 0.7$ mm for the element, ΔZ is the maximum deviation from the average plane at the rock scale and ΔZ_{el} that at the element scale. Indeed, a self-affine figure remains the same when scaled in different proportions in the different directions. This implies to make assumptions about the scaling ratio to use a self-affine description. Using morphological data of both rock walls (x, y and z coordinates see Fig. 8c), the maximum deviation for both rock walls is calculated and the maximum deviation is estimated from Eq. (5). Then, the reduction of the mechanical aperture is considered to be $\Delta E_{el} = 2\Delta Z_{el}$. The calculation of ΔE_{el} as well as the calibration of the reduction function have been performed at $W = 4$ mm. This specific step has been chosen because of the flow repartition, which is highly anisotropic. ΔE_{el} has been found equal to 0.05 mm for $W = 4$ mm and it has been kept constant for all elements and shear steps.

3.2. Calculation of hydraulic aperture

The hydraulic aperture of the each element is calculated according to Eq. (6) proposed by Barton et al. [2]

$$e_{el}(\mu m) = \frac{\overline{JRC}_{el}^{2.5}}{\left(\frac{E_{el}}{e_{el}}\right)^2}, \quad (6)$$

where $\overline{JRC}_{el}$ is the average roughness of the element (micro-scale parameter), e_{el} the hydraulic aperture and E_{el} the mechanical aperture. Note that from a dimensional point of view, this empirical equation has to be multiplied by a length to be consistent. This length is considered herein to be equal to 1 μm. The equation is applicable when E_{el}/e_{el}. E_{el} and e_{el} values are expressed in microns.

3.3. Reduction function α

The permeability K of a porous medium can be empirically described as an exponential function of the porosity [42–44] as follow: $\log K = aP + b$, where P is the porosity of the medium (a and b are constant). Moreover, Patir and Cheng [45] have described the evolution of hydraulic aperture as an exponential function of the ratio between initial hydraulic aperture and the standard deviation at the macro-scale. Likewise, it assumed that the reduction function is an exponential function of the ratio $\Delta E_{el}/E_{el}$ so that it comes

$$\alpha = C_1 \exp^{-C_2(\Delta E_{el}/E_{el})}. \quad (7)$$

The reduction function α has been calibrated at shear step $W = 4$ mm in order to determine C_1 and C_2 according to the calibration procedure shown in Fig. 9. The model counts thousands of elements, making the calibration of each coefficient of permeability very difficult. The solution chosen for the calibration has been a repartition of all elements in eight classes having an interval of 0.2 mm, value allowing a compromise between accuracy and feasibility (Fig. 10). This solution leads to eight values of coefficient of permeability to be calibrated manually as shown in Table 2. For class I, the average mechanical aperture is smaller than the ΔE_{el} so that the reduction function is based on seven classes only (II to VIII). Justification of this choice and results of the calibration are presented in the results section.

3.4. Comparison with the Reynolds equation

The model developed in this paper has been compared to the Reynolds equation in order to assess its efficiency (see [17] for details on Reynolds equation). If there is no

Please cite this article as: Giacomini A, et al. Numerical study of flow anisotropy within a single natural rock joint. Int J Rock Mech Mining Sci (2007), doi:10.1016/j.ijrmms.2007.04.007

internal source or sink, the Reynolds equation can be written as

$$\frac{\partial}{\partial x}\left(\frac{\rho g e^3(x,y)}{12\mu}\frac{\partial h}{\partial x}\right)+\frac{\partial}{\partial y}\left(\frac{\rho g e^3(x,y)}{12\mu}\frac{\partial h}{\partial y}\right)=0. \quad (8)$$

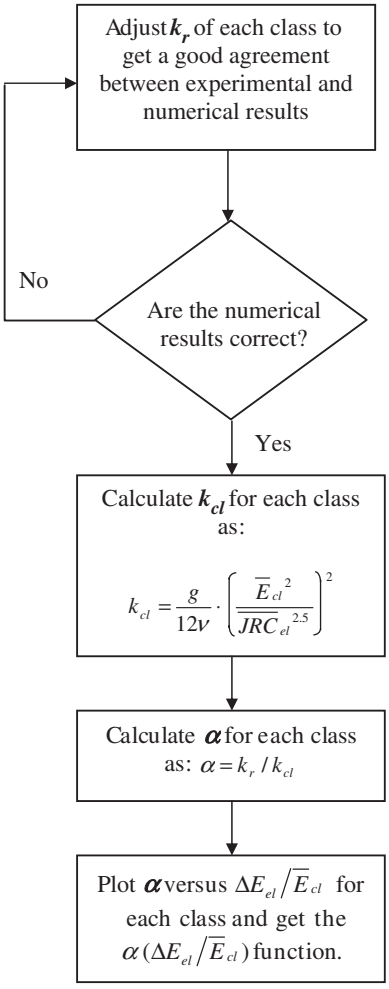

Fig. 9. Flow chart of the calibration procedure for the reduction function $\alpha(\Delta E_{el}/\overline{E}_{cl})$.

Darcy's law combined with the continuity equation for a 2D problem gives

$$\frac{\partial}{\partial x}\left(k_x\frac{\partial h}{\partial x}\right)+\frac{\partial}{\partial y}\left(k_y\frac{\partial h}{\partial y}\right)=0. \quad (9)$$

The Reynolds equation has been solved in Abaqus giving to each element a coefficient of permeability equal to

$$k_x=k_y=\frac{\rho g e^3}{12\mu}. \quad (10)$$

With such a value of coefficient of permeability Eq. (9) can be turned into Eq. (8).

4. Results

4.1. Calibration of the reduction function

The model developed herein is denoted MR (for micro-roughness). During the calibration phase, the coefficients of permeability of the classes are chosen in order to obtain flow rates as close as possible to the experimental values (see Fig. 9). Table 2 shows the average mechanical aperture for each class of the calibration model, the corresponding hydraulic aperture and the calibrated coefficient of

Table 2
Definition of element classes for the calibration: intervals of mechanical aperture and average mechanical aperture of each class $\overline{E}_{cl}$, average class hydraulic aperture $\overline{e}_{cl}$ and reduced coefficient of permeability k_r calibrated manually

Class	Interval of $\overline{E}_{el}$	$\overline{E}_{cl}$ (mm)	$\overline{e}_{cl}$ (mm)	k_r (m/s)
I	$\overline{E}_{el}\leqslant 0.0002$ mm	0.0001	3.49E-09	1.0E-38
II	$0.0002\,\text{mm}<\overline{E}_{el}<0.2$ mm	0.099	3.42E-03	1.0E-33
III	$0.2\,\text{mm}<\overline{E}_{el}<0.4$ mm	0.304	3.23E-02	1.0E-13
IV	$0.4\,\text{mm}<\overline{E}_{el}<0.6$ mm	0.5	8.73E-02	1.0E-9
V	$0.6\,\text{mm}<\overline{E}_{el}<0.8$ mm	0.695	1.69E-01	8.0E-6
VI	$0.8\,\text{mm}<\overline{E}_{el}<1.2$ mm	0.973	3.31E-01	2.0E-3
VII	$1.2\,\text{mm}<\overline{E}_{el}<1.4$ mm	1.285	5.77E-01	23.0E-3
VIII	$1.4\,\text{mm}<\overline{E}_{el}$	1.751	1.07E+00	178.0E-3

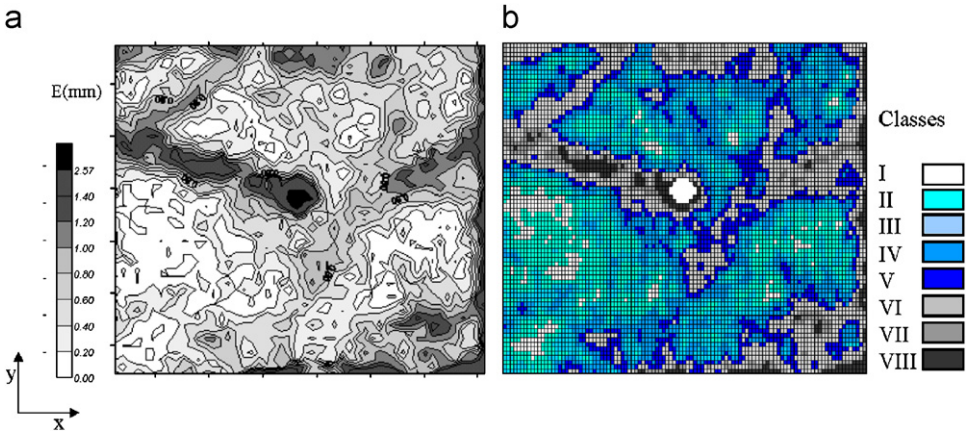

Fig. 10. (a) Representation of the experimental void map (data after [1]) and (b) classes model subdivision used for the calibration ($W=4$ mm).

permeability. Note that if the reduction in mechanical aperture ΔE_{el} is greater than the value of mechanical aperture E_{el}, the mechanical aperture considered is equal to ΔE_{el}, which leads to the maximum reduction function. Fig. 11a shows the distribution of flow rates for the calibration model (with classes) and for model MR using the calibration obtained (without classes). Experimental values are plotted as well. It has to be noticed that the approach followed to describe the micro-scale effect enables a good reproduction of the flow anisotropy meaning that the physical phenomenon is properly modelled. Indeed, numerical results of both models are very close to the experimental values. Fig. 11b shows the flow rates ratio Q_{MR}/Q_{exp} and $Q_{calibration}/Q_{exp}$ in each sector of the rock joint. It can be concluded that organizing the elements by classes does not affect much the flow rates values and distribution. The solution adopted for the calibration is then validated. The calibration of the reduction function is reported in Fig. 12. It can be seen that the points obtained are not excessively scattered and the exponential law used for the reduction function fits properly the results ($R^2 = 0.991$). C_1 has been found equal to 2.95 and C_2 equal to 131.78; see Eq. (7). Then, α is defined as

$$\alpha = 2.95 \exp^{-131.78(\Delta E_{el}/E_{el})}. \quad (11)$$

4.2. Results of the model

Fig. 13a and b show the distribution of water within the rock joint at $W = 4$ mm for model MR and Reynolds equation. With the micro-scale effects of model MR, water flows in the more opened channels (three channels identified and visible Fig. 10), whereas water flows also in other zones of the joint for the Reynolds equation. For model MR, the maximum fluid velocity is reached in the major channel located at the border between sectors 1 and 5 and is about 2 m/s. In the two minor channels, the fluid velocity is found equal to 0.03 m/s. In comparison, Reynolds equation gives much higher fluid velocity in the major channel (90 m/s) due to the relatively high permeability of the elements. Indeed, Fig. 14 shows the statistical distribution of the permeability ratio k_R/k_{MR}, k_R being the coefficient of permeability used to implement the Reynolds equation and k_{MR} being the coefficient of permeability for the model MR. It can be noticed that the coefficient of permeability used for the Reynolds equation is in average

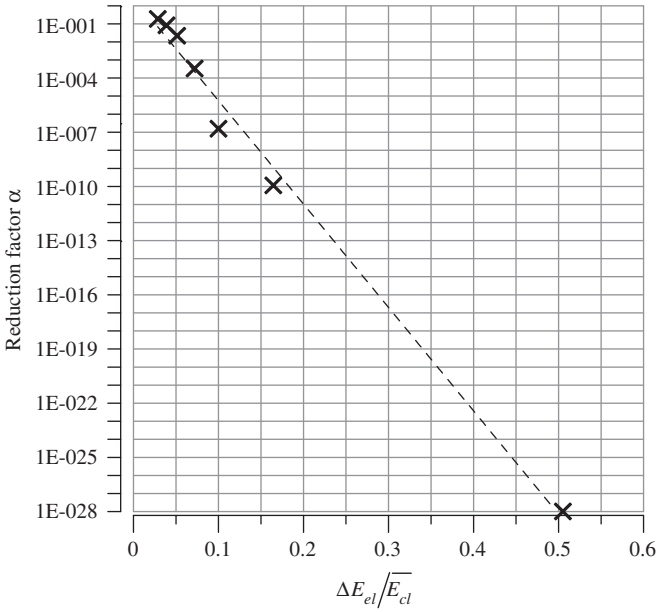

Fig. 12. Calibration of the reduction function: α and $\Delta E_{el}/\overline{E}_{cl}$ have been plotted for each class (logarithmic scale for α). The dot line represents the interpolation law: $\alpha = 2.95 \exp^{-131.78(\Delta E_{el}/\overline{E}_{cl})}$ ($R^2 = 0.991$).

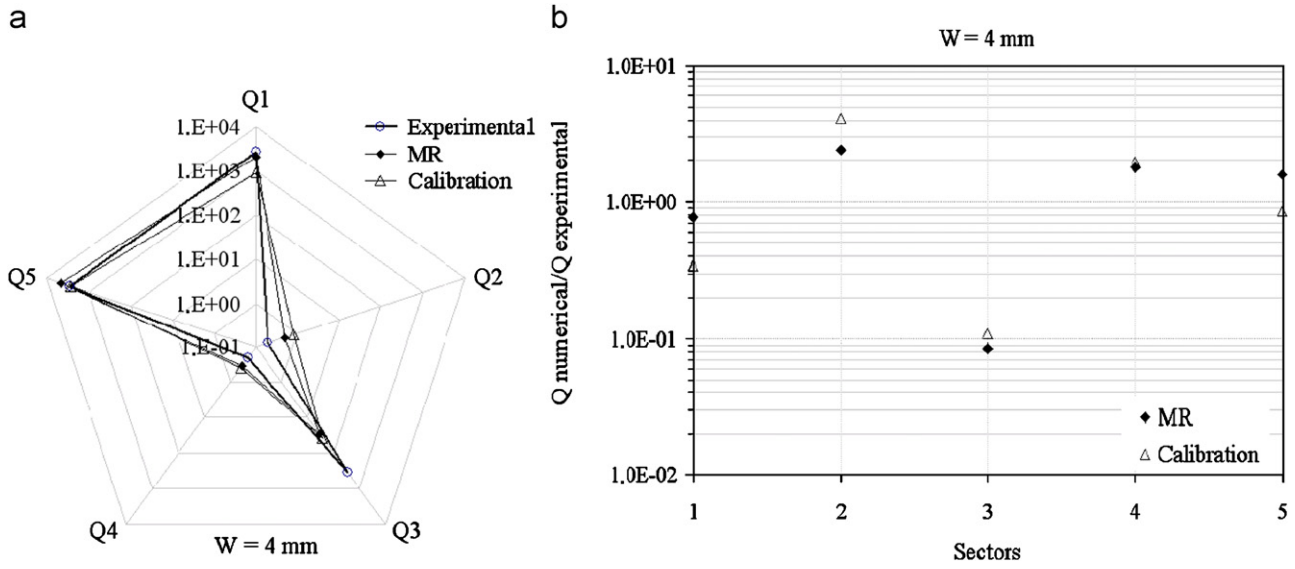

Fig. 11. (a) Experimental and numerical flow rates values for the calibration and model MR at $W = 4$ mm and (b) flow rate ratio Q_{MR}/Q_{exp} and $Q_{calibration}/Q_{exp}$ for each sector.

Please cite this article as: Giacomini A, et al. Numerical study of flow anisotropy within a single natural rock joint. Int J Rock Mech Mining Sci (2007), doi:10.1016/j.ijrmms.2007.04.007

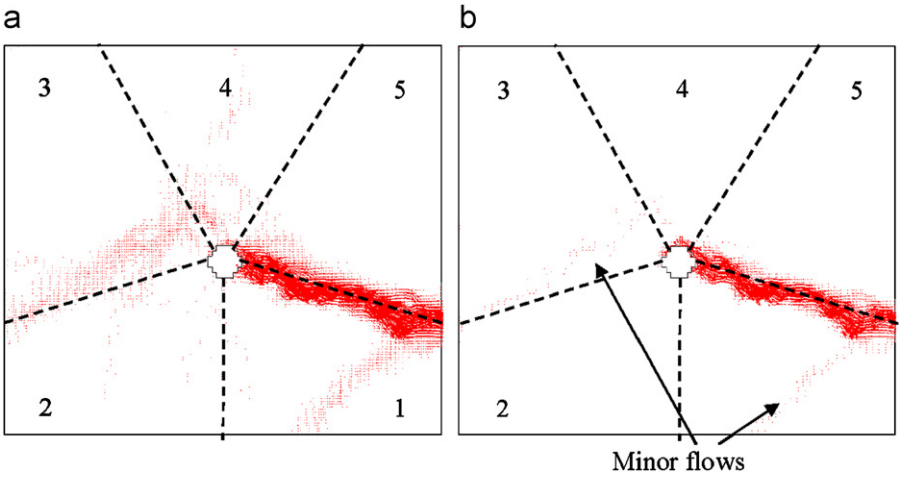

Fig. 13. Distribution of water within the rock joint for Reynolds equation (a) and model MR (b). $W = 4$ mm. Dot lines are the representation of the sectors but effective division of each sector is at the outlet of the joint.

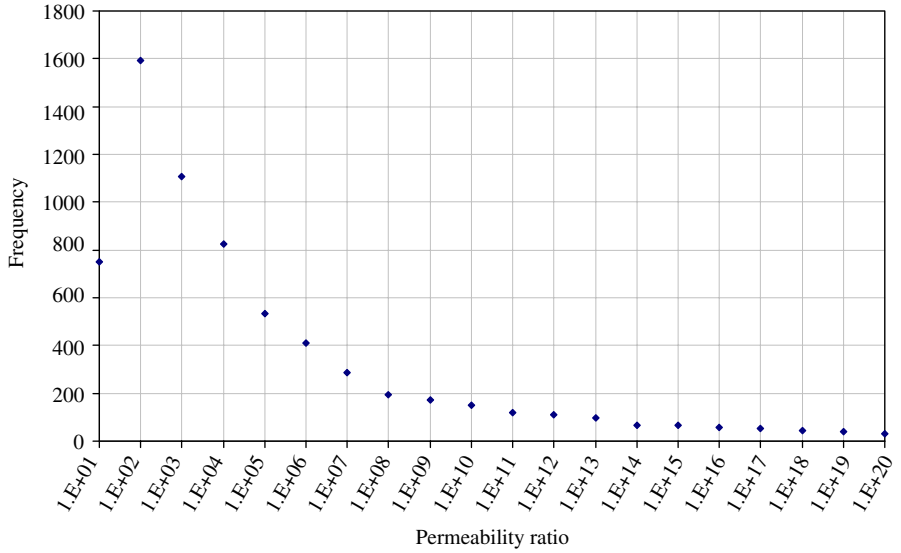

Fig. 14. Statistical distribution of permeability ratio k_R/k_{MR} for all the elements, k_R: coefficient of permeability corresponding to the Reynolds equation. k_{MR}: coefficient of permeability for the model MR $W = 4$ mm.

1000 greater than that of model MR. The ratio reaches values as high as 1×10^{20} due to the drastic reduction of the coefficient of permeability allowed by the reduction function α. By dropping the coefficient of permeability of the smallest elements, the reduction function tends to localize the flow in the elements of highest coefficient of permeability, corresponding to the most opened zones. The flow anisotropy is then properly reproduced, whereas Reynolds equation does not capture the anisotropy (Fig. 15a) and overestimates the flow (Fig. 15b). Figs. 16–19 show experimental and numerical flow rates (in logarithmic scale) as well as flow rate ratios, which are relevant to assess the efficiency of both models. At the beginning of the test ($W = 2$ mm), experimental data show water flowing in almost all the sectors except sector 3. However, a quite significant channel leading to sector 3 and visible in Fig. 10 is also present at $W = 2$ mm [1]. The absence of flow in sector 3 could be due to some gouge material produced during the first 2 mm of shear displacement and obstructing existing channels. The numerical results (both MR and Reynolds equation) show an isotropic distribution of the flow with values much higher than the experimental results. Compared to the model MR, Reynolds equation overestimates by two orders of magnitude the values of flow rates as shown in Fig. 16b. For $W = 6$ mm (Fig. 17), experimental flow in sector 1 decreases while other sectorial flows are almost constant. Model MR is still very close to the experimental data even if a slight increase in sector 4 is shown. The experimental reorganization of the flow depends also on the production and evacuation of gouge material, which is difficult to capture in a model. Prediction of Reynolds equation is still isotropic and overestimated. This can be seen properly in Fig. 17b, where the flow ratio for model MR is close to 1

Please cite this article as: Giacomini A, et al. Numerical study of flow anisotropy within a single natural rock joint. Int J Rock Mech Mining Sci (2007), doi:10.1016/j.ijrmms.2007.04.007

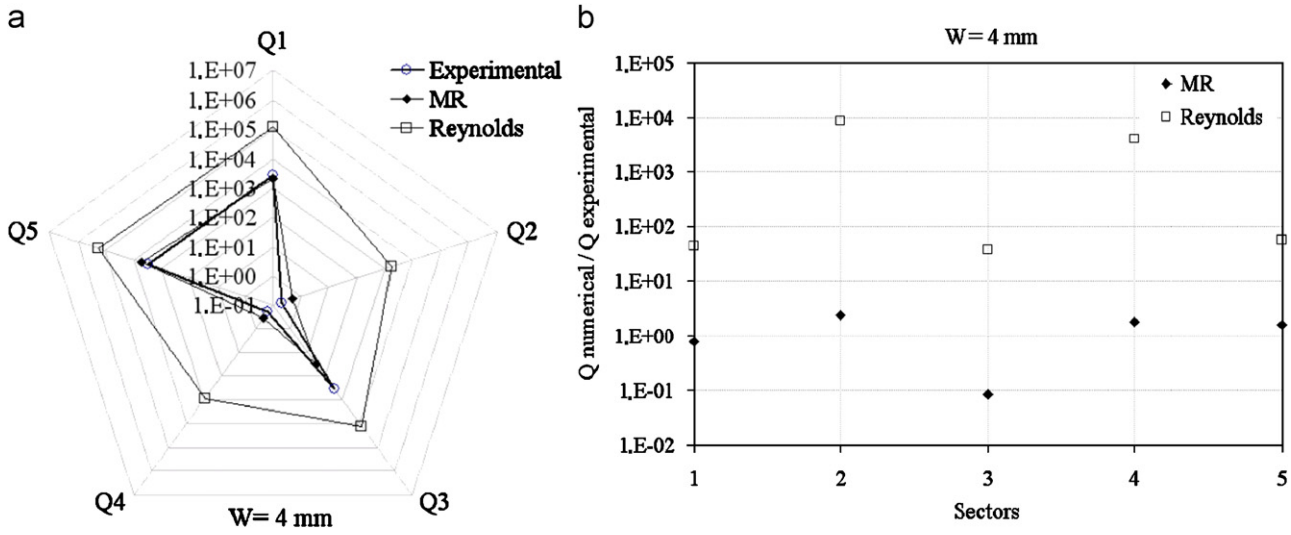

Fig. 15. (a) Experimental and numerical flow rates values and (b) flow rate ratio Q_{MR}/Q_{exp} and Q_R/Q_{exp} for each sector $W = 4$ mm.

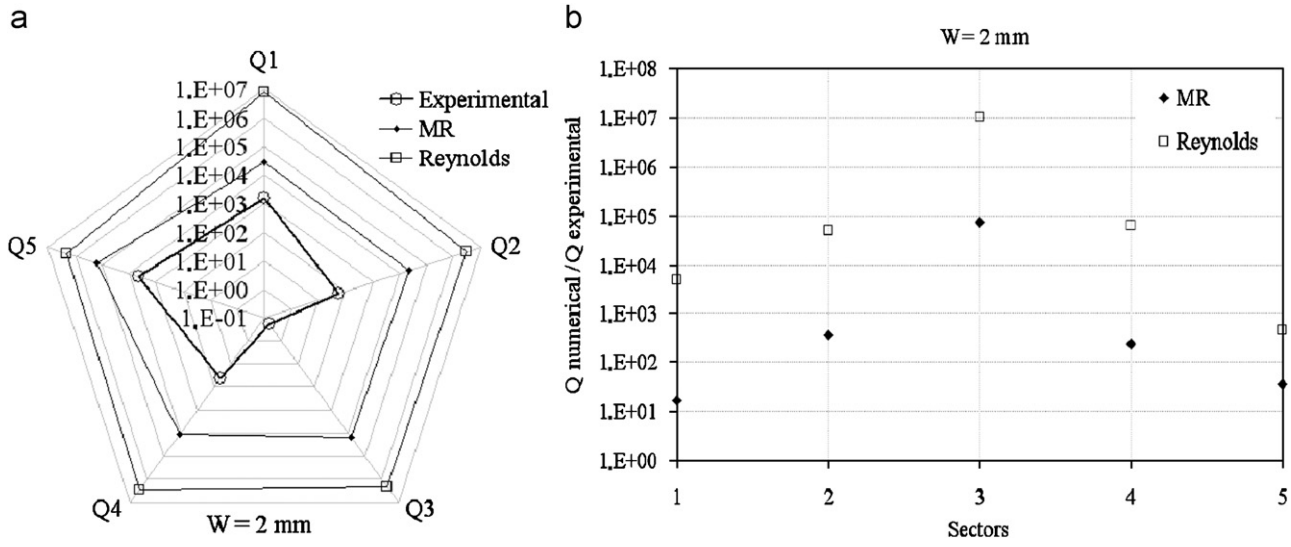

Fig. 16. (a) Experimental and numerical flow rates values and (b) flow rate ratio Q_{MR}/Q_{exp} and Q_R/Q_{exp} for each sector $W = 2$ mm.

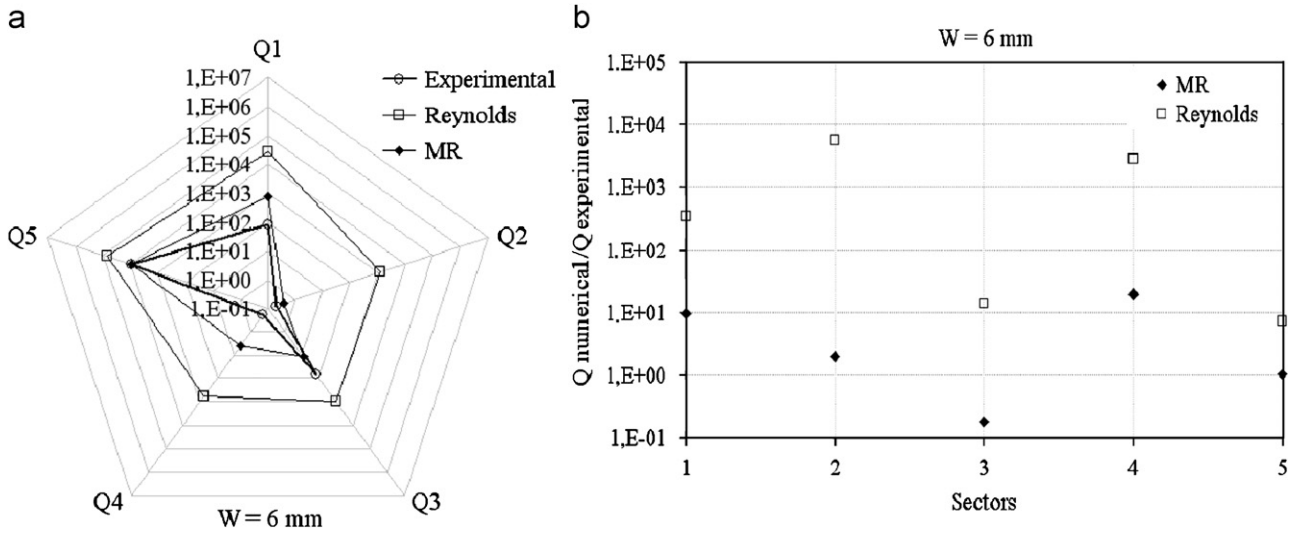

Fig. 17. (a) Experimental and numerical flow rates values and (b) flow rate ratio Q_{MR}/Q_{exp} and Q_R/Q_{exp} for each sector $W = 6$ mm.

Please cite this article as: Giacomini A, et al. Numerical study of flow anisotropy within a single natural rock joint. Int J Rock Mech Mining Sci (2007), doi:10.1016/j.ijrmms.2007.04.007

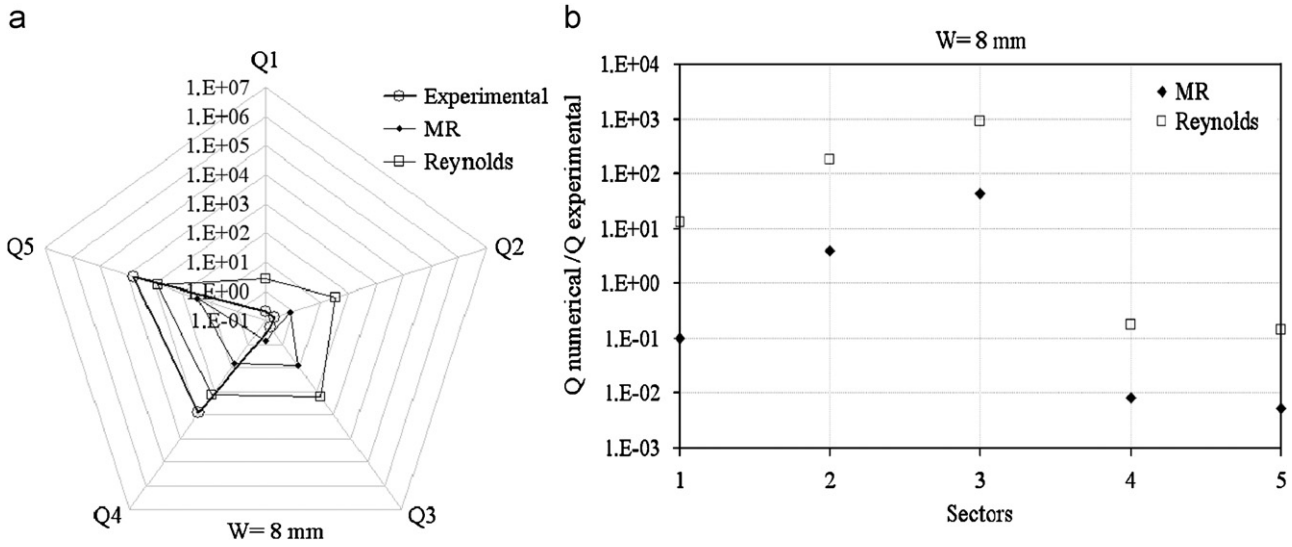

Fig. 18. (a) Experimental and numerical flow rates values and (b) flow rate ratio Q_{MR}/Q_{exp} and Q_R/Q_{exp} for each sector $W = 8$ mm.

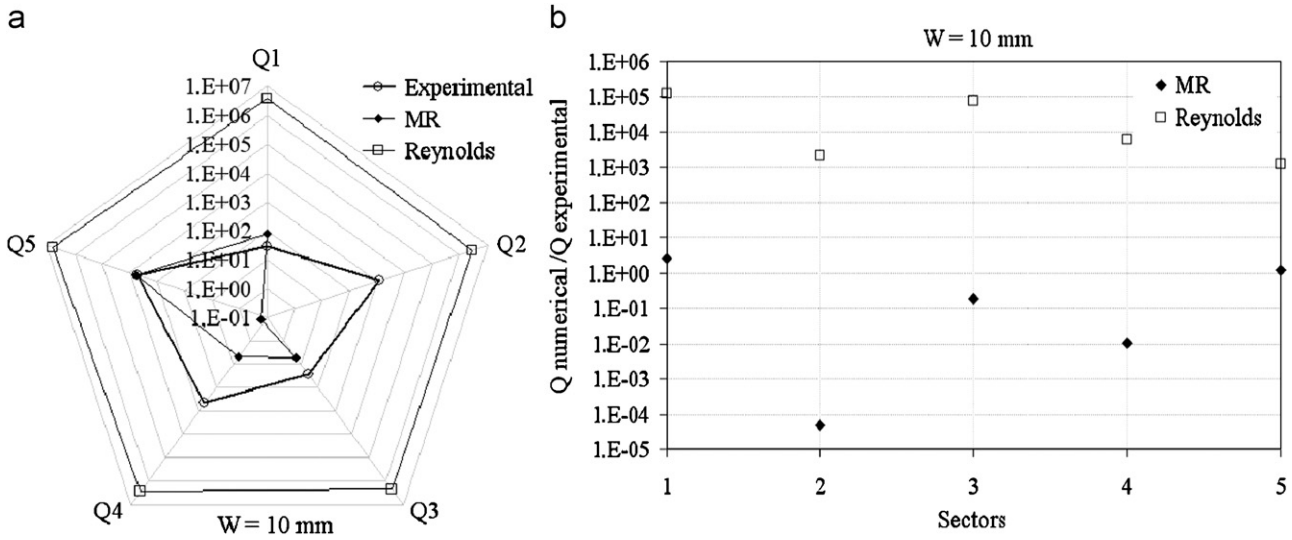

Fig. 19. (a) Experimental and numerical flow rates values and (b) flow rate ratio Q_{MR}/Q_{exp} and Q_R/Q_{exp} for each sector $W = 10$ mm.

with a maximum ratio of 20 for sector 4, whereas flow ratio for Reynolds equation reaches 6000. At $W = 8$ mm, there is a modification of flow anisotropy corresponding to a change of the void space and a reorganization of channels. Flow is highly anisotropic since water flows mainly in sectors 4 and 5. At this stage, Fig. 18a shows that both Reynolds equation and model MR provide reasonable values of flow rate. Fig. 18b enables to better assess the results. It can be seen that model MR gives a better prediction for sectors 2 and 3, whereas Reynolds equation results are better than model MR for sector 4 and 5. At the end of the experimental shear test ($W = 10$ mm), water has been found to flow in all sectors. Model MR gives a relatively good agreement between numerical and experimental results: three out of five values of flow rates are exact. The difference in the other sectors (2 and 4) comes from the fact that the model does not take into account phenomena such as asperities degradation and gouge material production. So far, no publication related to a model taking into account such phenomenon has been found by the authors in the technical literature. Reynolds equation is far away from the experimental results as confirmed by flow ratio in Fig. 19b. As a conclusion, on the 25 flow rates ratios analysed (five steps and five sectors), the model MR developed herein gives a better prediction than Reynolds equation in 20 cases, Reynolds equation is better than MR in three cases ($W = 8$ mm, sectors 4 and 5; $W = 10$ mm, sector 2) and two cases are equal ($W = 6$ mm, sector 3; $W = 8$ mm, sector 1).

4.3. Flow regime

Hans [1] has performed a hydraulic excursion at each step of shear displacement in order to investigate the flow

Please cite this article as: Giacomini A, et al. Numerical study of flow anisotropy within a single natural rock joint. Int J Rock Mech Mining Sci (2007), doi:10.1016/j.ijrmms.2007.04.007

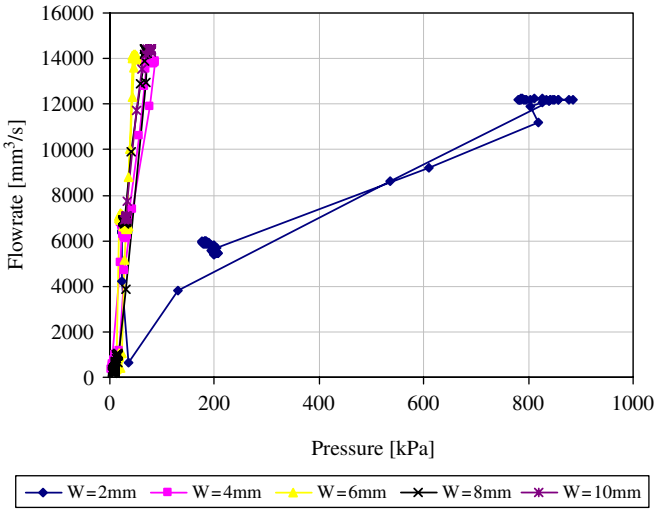

Fig. 20. Experimental results of the hydraulic excursions: evolution of flow rate versus injection pressure for $W = 0$–10 mm.

regime. Such excursion means a successive increase and decrease of the injection pressure to observe the hydraulic response of the joint in terms of flow rate. The evolution of flow rate versus injection pressure gives information about the flow regime: a linear evolution means laminarity, whereas a non-linear evolution corresponds to turbulence. The results are given in Fig. 20. A linear evolution of flow rate versus injection pressure can be seen for W ranging from 4 to 10 mm. The flow seems to be turbulent at $W = 2$ mm (non-linear evolution). The model MR is based on Darcy's law that assumes a laminar flow. Since the numerical values of flow rate are very close to the experimental results, the numerical flow is considered to be laminar such as the experimental flow.

5. Conclusions

The flow within a rock joint is governed by Navier–Stokes equations, which are quite difficult to solve. The simplest approximation of Navier–Stokes equation is the cubic law, which is known to not reproduce properly the flow distribution. The Reynolds equation is another approximation of the Navier–Stokes equations, which is easy to implement and considered, so far, to better reproduce the flow anisotropy. The model developed in this paper is based on the cubic law and on a reduction function depending on the micro-roughness of the joint. The effect provided by the reduction function is to drop drastically the coefficient of permeability of the smallest elements tending to localize the flow in the most opened channels. The numerical results have been compared to experimental data due to Hans [1] and to the Reynolds equation. It has been shown that the model developed herein reproduces quite properly the flow anisotropy and gives realistic values of fluid velocities. The production and evacuation of gouge material has a significant influence on the reorganization of the flow during the shear tests. The model MR does not capture this phenomenon so that, the evolution of flow rates during the shear tests is not perfect. However, the predictions given by model MR are better than that of Reynolds equation in 20 out of 25 cases. Finally, the model is based on Darcy's law, which assumes a laminar flow. Experimental evidence of flow laminarity and considerations of orders of magnitude are used to justify the use of Darcy's law.

Acknowledgements

The authors thank Marc Boulon and Julien Hans of the Laboratory Soils, Solids, Structures of the University Joseph Fourier in Grenoble (France) for providing experimental data support. They also thank Kristian Krabbenhoft from the Centre for Geotechnical and Materials Modelling, University of Newcastle, for fruitful scientific discussions on finite elements.

References

[1] Hans J. Etude expérimentale et modélisation numérique multiéchelle du comportement hydromécanique des répliques de joints rocheux. PhD thesis, Joseph Fourier University, Grenoble, France, 2002.
[2] Barton N, Bandis S, Bakhtar K. Strength, deformation and permeability of rock joints. Int J Rock Mech Min Sci Geomech Abstr 1985;22:121–40.
[3] Barton N. Modelling rock joint behaviour from in situ block tests: implication for nuclear waste repository design. Office of Nuclear Waste Isolation, Columbus, Ohio, ONWI-308, 1982, 96pp.
[4] Barton N. Review of a new shear strength criterion for rock joints. Eng Geol 1976;7:287–332.
[5] Gale JE. Assessing the permeability characteristics of fractured rock. Geol Soc Am Spec Paper 1982;189:163–80.
[6] Raven KG, Gale JE. Water flow in a natural rock fracture as a function of stress and sample size. Int J Rock Mech Min Sci Geomech Abstr 1985;22:251–61.
[7] Lee HS, Cho TF. Hydraulic characteristics of rough fractures in linear flow under normal and shear load. Rock Mech Rock Eng 2002;35(4):299–318.
[8] Pyrak-Nolte LJ, Morris JP. Single fracture under normal stress: the relation between fracture specific stiffness and fluid flow. Int J Rock Mech Min Sci 2000;37:245–62.
[9] Pyrak-Nolte LJ, Myer LR, Cook NGW, Witherspoon PA. Hydraulic and mechanical properties of natural fractures in low permeability rock. In: Proceedings of the sixth international congress rock mechanics. Montreal, 1987, pp. 225–31.
[10] Pyrak-Nolte LJ, Cook NGW, Nolte D. Fluid percolation through single fractures. Geophys Res Lett 1988;15(11):1247–50.
[11] Barton N. A relationship between joint roughness and joint shear strength. In: Proceedings of the international symposium on rock fracture. Nancy, France, 1971, p. 1–8.
[12] Marache M, Riss J, Gentier S, Chilès JP. Characterization and reconstruction of a rock fracture surface by geostatistcs. Int J Numer Anal Meth Geomech 2002;26:873–96.
[13] Tse R, Cruden DM. Estimating joint roughness coefficient. Int J Rock Mech Min Sci 1979;16:303–7.
[14] Kulatilake PHSW, Balasingam P, Park J, Morgan R. Natural rock joint roughness quantification through fractal techniques. Geotech Geol Eng 2006;24:1181–202.
[15] Turk N, Greig MI, Dearman WR, Amin FF. Characterization of rock joint surfaces by fractal dimension. In: Farmer IW, Daemen J, Desai CS, Glass CE, Neuman SP, editors. Proceedings of the 28th US

symposium on rock mechanics, Tucson, Arizona. Rotterdam: Balkema; 1987. p. 1223–36.
[16] Grasselli G, Wirth J, Egger P. Quantitative three-dimensional description of a rough surface and parameter evolution with shearing. Int J Rock Mech Min Sci 2002;39:789–800.
[17] Yeo IW, De Freitas MH, Zimmerman RW. Effect of shear displacement on the aperture and permeability of a rock fracture. Int J Rock Mech Min Sci 1998;35(8):1051–70.
[18] Bandis SC, Makurat A, Vik G. Predicted and measured hydraulic conductivity of rock joints. In: Proceedings of the international symposium fund rock joints. Bjorkliden, 1985, p. 269–80.
[19] Boulon MJ, Selvadurai APS, Benjelloun H, Feuga B. Influence of rock joint degradation on hydraulic conductivity. Int J Rock Mech Min Sci Geomech Abstr 1993;30:1311–7.
[20] Nguyen TS, Selvadurai APS. A model for coupled mechanical and hydraulic behaviour of a rock joint. Int J. Numer Anal Meth Geomech. 1998;22:29–48.
[21] Olsson R, Barton N. An improved model for hydromechanical coupling during shearing of rock joints. Int J Rock Mech Min Sci 2001;38:317–29.
[22] Archambault G, Gentier S, Riss J, Flamand R. The evolution of void spaces (permeability) in relation with rock joint shear behaviour. Int J Rock Mech Min Sci 1997;34(3–4):014.
[23] Brown SR. Fluid flow through rock joints: the effect of surface roughness. J Geophys Res 1987;92:1337–47.
[24] Zimmerman RW, Yeo IW. Fluid flow in rock fractures: from the Navier–Stokes equations to the cubic law. In: Dynamics of fluids in fractured rock, geophysical monograph 122, American Geophysics Union, Washington, 2000, p. 213–24.
[25] Snow DT. A parallel plate model of fractured permeable media. PhD thesis, University of California, Berkeley, 1965.
[26] Yasuhara H, Polak A, Mitani Y, Grader AS, Halleck P, Elsworth D. Evolution of fracture permeability through fluid-rock reaction under hydrothermal conditions. Earth Planet Sci Lett 2006;244:186–200.
[27] Sisavath S, Al-Yaarubi A, Pain C, Zimmerman RW. A simple model for deviation from the cubic law for a fracture undergoing dilation or closure. Pure Appl Geophys 2003;160:1009–22.
[28] Witherspoon PA, Wang JSY, Iwai K, Gale JE. Validity of cubic low for fluid flow in a deformable rock fracture. Water Resour Res 1980;16(6):1016–24.
[29] Chen Z, Narayan SP, Yang Z, Rahman SS. An experimental investigation of hydraulic behaviour of fractures and joints in granitic rock. Int J Rock Mech Min Sci 2000;37:1061–71.
[30] Lomize GM. Water flow through jointed rock. Moscow: Gosenergoizdat; 1951.
[31] Louis C. A study of groundwater flow in jointed rock and its influence on the stability of rock masses. Imperial college rock mechanical research report, 1969, 90pp.
[32] Louis C. Rock hydraulics in rock mechanics. In: Mŭller L, editor, CISM, Udine, 1974, p. 299–387.
[33] Zimmerman RW, Bodvarsson GS. Hydraulic permeability of rock fractures. Transp Porous Media 1996;23:1–30.
[34] Zimmerman RW. Fluid flow in rock fractures. In: Proceedings of the 11th international symposium of International Association for Computational Mathematics in Advanced Geomechanics, 2005, p. 89–107.
[35] Hans J, Boulon M. A new device for investigating the hydro-mechanical properties of rock joints. Int J Numer Anal Meth Geomech 2003;27:513–48.
[36] ABAQUS/Standard Version 6.4. ABAQUS Theory Manual. ABAQUS; 2004.
[37] ABAQUS/Standard Version 6.4. ABAQUS User's Manual. ABAQUS; 2004.
[38] Giacomini A. Caratterizzazione geomeccanica ed idraulica di masse rocciose discontinue. PhD thesis, Parma Univ, Parma, Italy, 2003.
[39] Chiara M. Studio teorico sperimentale per la valutazione della resistenza a taglio di discontinuità in roccia. MS thesis, Politecnico di Torino, Torino, Italy, 2000.
[40] Bandis S, Lumsden AC, Barton NP. Experimental studies of the shear behaviour of rock joints. Int J Rock Mech Min Sci 1981;18:1–21.
[41] Giani GP, Ferrero AM, Passarello G, Reinaudo L. Scale effect evaluation on natural discontinuity shear strength. In: Proceedings of the international congress fractured jointed rock mass. Lake Tahoe, California, 1992, p. 456–62.
[42] Dasgupta R, Roy S, Tarafdar S. Correlation between porosity, conductivity and permeability of sedimentary rocks—a ballistic deposition model. Physica A 2000;275:22–32.
[43] Luping T, Nilsson LO. A study of the quantitative relationship between permeability and pore size distribution of hardened cement pastes. Cement Concr Res 1992;22:541–50.
[44] Ollivier JP, Massat M. Permeability and microstructure of concrete: a review of modelling. Cement Concr Res 1992;22:503–14.
[45] Patir N, Cheng HS. An Average model for determining effects on three-dimensional roughness on partial hydrodynamic lubrication. J Lubr Tech 1978;100:12–7.

Please cite this article as: Giacomini A, et al. Numerical study of flow anisotropy within a single natural rock joint. Int J Rock Mech Mining Sci (2007), doi:10.1016/j.ijrmms.2007.04.007